Engineering 23 (2023) 56–63

Contents lists available at ScienceDirect

Engineering

journal homepage: www.elsevier.com/locate/eng

Research
Materials for Molecular Separations—Article

Robust Metal–Organic Frameworks with High Industrial Applicability in Efficient Recovery of C_3H_8 and C_2H_6 from Natural Gas Upgrading

Shikai Xian [a,b], Junjie Peng [c], Haardik Pandey [d], Timo Thonhauser [d], Hao Wang [a,*], Jing Li [a,b,*]

[a] Hoffmann Institute of Advanced Materials, Shenzhen Polytechnic, Shenzhen 518055, China
[b] Department of Chemistry and Chemical Biology, Rutgers University, Piscataway, NJ 08854, USA
[c] School of Chemistry and Chemical Engineering, South China University of Technology, Guangzhou 510640, China
[d] Department of Physics & Center for Functional Materials, Wake Forest University, Winston-Salem, NC 27109, USA

ARTICLE INFO

Article history:
Received 31 March 2022
Revised 27 June 2022
Accepted 13 July 2022
Available online 18 September 2022

Keywords:
Metal–organic framework
Hydrocarbon adsorption and separation
Selectivity
Stability
Scale-up synthesis

ABSTRACT

Developing efficient adsorbents with high uptake and selectivity for separation and recovery of C_2H_6 and C_3H_8 from natural gas is an important but challenging task. In this work, we demonstrate that high surface polarity and suitable pore diameter are two key factors that can synergistically enhance the separation performance, exemplified by metal–organic framework (MOF)-303 and Matériaux de l'Institut Lavoisier (MIL)-160, both possessing one-dimensional (1D) open channels with high density of heteroatoms and desired pore size (5–7 Å). Significantly, the uptake of MOF-303 for C_3H_8 is up to 3.38 mmol·g^{-1} at 298 K and 5 kPa with a record-high C_3H_8/CH_4 (5:85, v/v) ideal adsorbed solution theory (IAST) selectivity of 5114 among all reported MOFs. In addition, MOF-303 also displays high C_2H_6 uptake capacity (at 10 kPa) and C_2H_6/CH_4 (10:85, v/v) selectivity, reaching 1.59 mmol·g^{-1} and 26, respectively. Owing to the larger pore diameter and lower density of heteroatoms within its 1D channels, MIL-160 shows apparently lower uptake and selectivity compared to those of MOF-303, though the values exceed those of majority of reported MOFs. Density functional theory (DFT) calculations verify that the high surface polarity and the suitable pore diameter synergistically enhance the affinity of the frameworks toward C_3H_8 and C_2H_6, giving rise to the high loading capacity and selectivity for C_3H_8 and C_2H_6. Both MOFs feature remarkable moisture stability without structural change upon exposure to 95% relative humidity (RH) for a month. In addition, synthesis of both compounds can be readily scaled up through one-pot reactions to afford about 5 g samples with high crystallinity. Finally, the substantial potential of MOF-303 and MIL-160 as advanced adsorbents for efficient separation of $C_3H_8/C_2H_6/CH_4$ has been demonstrated by ternary breakthrough experiments, regeneration tests, and cyclic evaluation. The excellent separation performance, high stability, low cost, and good scalability endow both MOFs promising adsorbents for natural gas purification and recovery of C_2H_6 and C_3H_8.

1. Introduction

As the result of rapid urbanization, industrialization, and human population growth, the consumption of fossil fuels has been increasing constantly and swiftly. Natural gas is one of the most commonly used energy sources not only due to its abundant reserves in nature but also because it is more eco-friendly compared to oil and coal [1,2]. Generally, besides CH_4 as the main component, C_2H_6 (0–20%) and C_3H_8 (0–5%) coexist in the natural gas and should be fully recovered individually for updating the quality of natural gas. Subsequently, the recovered C_2H_6 and C_3H_8 can be utilized to produce C_2H_4 and C_3H_6 through catalytic dehydrogenation, which are the raw materials for producing various plastics, such as polyethylene, poly (vinyl chloride), and polypropylene [3–5]. Traditional cryogenic distillation has shown excellent performance in industrial separation processes but it is operated under high pressure and/or low temperature, leading to high energy-consumption [6,7]. Among the newly developed separation methods, adsorptive separation technology has been regarded as a promising alternative to cryogenic distillation because of its high separation efficiency and low energy input

* Corresponding authors.
E-mail addresses: haowang18@foxmail.com (H. Wang), jingli@rutgers.edu (J. Li).

https://doi.org/10.1016/j.eng.2022.07.017

[8,9]. The applicability of adsorptive separation is largely dependent on the performance of adsorbents, which involves their porosity, pore dimensions, and pore surface functionality.

Metal–organic frameworks (MOFs) represent an emerging class of porous materials assembled from metal centers and organic ligands through coordination bonds, which have drawn tremendous attention in the field of gas separation, due to their intrinsic advantages including extra-high surface area, structural diversity, pore tunability, and controllable functionality [10–14]. While MOFs have shown encouraging potential in the separation and recovery of C_2H_6 and C_3H_8 from natural gas, there still exist several problems that need to be addressed. First, the uptake capacity of C_2H_6 and C_3H_8 at low pressure is still not sufficient. For example, boron cage pillared supramolecular metal–organic framework (BSF)-2 possesses a very high selectivity but the equilibrium uptake amounts of C_3H_8 and C_2H_6 are only 1.77 and 1.22 $mmol \cdot g^{-1}$, respectively, leading to low separation efficiency [15]. Matériaux de l'Institut Lavoisier (MIL)-100(Fe) exhibits high uptake capacity of C_2H_6 and C_3H_8 at 1 bar (1 bar = 10^5 Pa) but the values are too low at low pressure [16]. As a result, these MOFs show limited applicability due to the low C_2H_6 and C_3H_8 concentrations in nature gas. Low stability of most reported MOFs in the presence of moisture is the second problem. For example, MOF-74 and Hong Kong University of Science and Technology (HKUST)-1 feature high separation capability but suffer from structural decomposition in humid air [17,18]. High moisture stability is essential for an adsorbent to be used in nature gas purification because the gas mixture always contains a certain amount of water vapor [19–22]. In addition, material cost and scale-up capability are also important factors in determining the feasibility for industrial applications. While some MOFs show high performance and sufficient water/moisture stability, such as $Ni(TMBDC)(DABCO)_{0.5}$ (TMBDC: 2,3,5,6-tetramethylterephthalic acid; DABCO: 1,4-diazabicyclo [2.2.2]octane) [23] and Fujian Institute of Research on the Structure of Matter (FJI)-C4 [7], they are constructed from expensive organic linkers which would seriously hinder their industrial utility when considering the economic feasibility. MOFs synthesized in relative harsh conditions involving high temperature, high pressure, large amounts of template, or complex steps are usually difficult to scale up [24,25]. Hence, developing or screening ideal MOF adsorbents for targeted industrial applications require consideration of all these aspects in order to reach an optimal balance between separation performance, stability, and cost.

To improve the uptake of C_2H_6 and C_3H_8 at low pressure, we propose an effective strategy based on our previous study: simultaneously enhancing the polarity of the pore surface and tuning the pore diameter to a suitable size (Fig. 1). On one hand, increasing surface polarity by introducing polar atoms or functional groups could markedly strengthen the interaction between gas molecules and MOFs as the C–H bond in hydrocarbons preferentially binds to the polar atoms or functional groups through hydrogen bonds [11,26,27]. On the other hand, a suitable pore size is very crucial because the diffusion of C_3H_8 molecules would be seriously restricted if pore is too narrow, and on the contrary, a larger pore always causes weaker interaction, leading to unsatisfactory uptake capacity and selectivity, especially at low pressure. We could envision that suitable pore diameter and highly polar surface simultaneously existing in a MOF could concurrently reinforce multiple hydrogen bonds, resulting in significant enhancement in high adsorption capacity and selectivity. As to moisture stability, MOFs built on metals with high valence such as Zr^{4+}, Cr^{3+}, and Al^{3+} are generally resistant to water [28–32]. Finally, using MOFs with inexpensive ligands and high scale-up ability can lower the total cost and significantly enhance their likelihood for industrial applications.

MOF-303 and MIL-160 are selected in this work when taking all these factors into account. Their ultrahigh hydrothermal stability, large surface area, and especially the suitable pore diameter, as well as the high density of heteroatoms in the one-dimensional (1D) channel synergistically afford an intriguing performance in natural gas purification and recovery of C_2H_6 and C_3H_8. Adsorption isotherms for CH_4, C_2H_6, and C_3H_8 were determined by a volumetric method. The ideal adsorbed solution theory (IAST) selectivity of C_2H_6/CH_4, C_3H_8/CH_4, and C_3H_8/C_2H_6 at various ratios, as well as the isosteric heats of adsorption for all three gases were calculated. Ternary fixed-bed breakthrough experiments were carried out to further confirm their potential for real-world applications. Finally, density functional theory (DFT) calculation was applied to study the adsorption mechanism for CH_4, C_2H_6, and C_3H_8.

2. Materials and methods

2.1. Reagents and solvents

All reagents were purchased commercially and used as received. Aluminum chloride hexahydrate ($AlCl_3 \cdot 6H_2O$) was

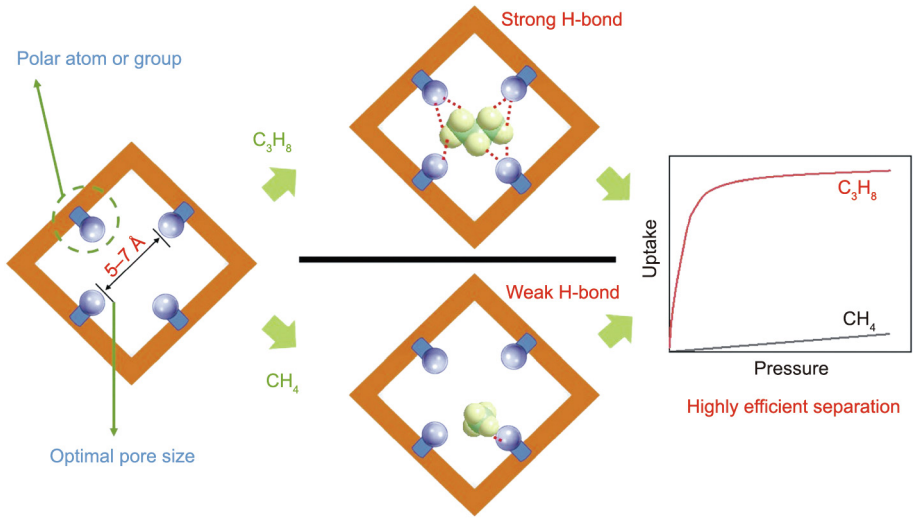

Fig. 1. Schematic illustration on how highly polar surface and suitable pore diameter of a MOF may synergistically enhance the affinity of the framework toward C_3H_8 to result in a highly efficient separation of C_3H_8 and CH_4.

purchased from Alfa Aesar (USA); 3,5-pyrazoledicarboxylic acid monohydrate (H_3PDC) and 2,5-furandicarboxylic acid were both supplied by TCI America (USA); sodium hydroxide (NaOH) was purchased from Acros Organics (USA); the high-purity gases for adsorption experiments were obtained from Praxair, Inc. (USA).

2.2. Preparation of MOF-303 and MIL-160

MOF-303 was prepared by using the procedure reported by Yaghi et al. [33] with some modifications. First, 1.04 g $AlCl_3{\cdot}6H_2O$ (4.308 mmol) and 0.75 g H_3PDC (4.308 mmol) were dissolved in 72 mL water in a 200 mL glass flask, 3 mL aqueous NaOH (0.26 g, 6.5 mmol) were added dropwise to the above mixture under stirring. The flask was then heated at 100 °C with reflux for 12 h. After cooling down to room temperature, the as-synthesized MOF-303 powder was obtained by filtration. To remove the remaining 3,5-pyrazoledicarboxylic acid, the powder was washed thoroughly with water, followed by heated under vacuum at 150 °C for 12 h. MIL-160 was synthesized by the same procedure as that of MOF-303 by replacing the ligand H_3PDC with 2,5-furandicarboxylic acid.

2.3. Characterization

Powder X-ray diffraction (PXRD) patterns were collected on a Bruker D8 Venture X-ray diffractometer (Bruker, USA) with a 2θ range of 3°–35° at 2.0(°)·min^{-1}. Thermogravimetric (TG) measurements were performed on a TA Q-5000 apparatus (TA Instruments, USA), with a ramping rate of 10 K·min^{-1} from ambient temperature to 973 K under a flowing nitrogen environment. Nitrogen (N_2) adsorption isotherms were obtained on a Micromeritics 3Flex analyzer (Micromeritics Instrument Corporation, USA) at 77 K. The Brunauer–Emmett–Teller (BET) model was chosen to evaluate the specific surface area, and the Horvath–Kawazoe (HK) method was conducted to acquire the micropore size distribution.

2.4. Adsorption experiments

CH_4, C_2H_6, and C_3H_8 adsorption isotherms were performed on the 3Flex analyzer. Volumetric sorption data were collected at varied temperatures and pressures up to 1 bar. Approximately 80–100 mg of sample were used and degassed at 423 K for 12 h prior to the adsorption experiments.

2.5. Breakthrough experiments

Breakthrough curves of a ternary mixture $CH_4/C_2H_6/C_3H_8$ (85:10:5, v/v/v) were obtained on a homemade experimental setup under the control of a mass flow meter, with the flow rate set to be 2 mL·min^{-1}. A small adsorption column was prepared by packing about 0.2 g of activated sample into a long stainless hollow cylinder. The real time concentration of the effluent component was monitored by gas chromatography (Agilent, USA). Before the experiment, the packed column was heated at 423 K under He flow (5 mL·min^{-1}) for 1 h. After the breakthrough experiment, the desorption curves were collected at 323 K under 5 mL·min^{-1} N_2 flow.

2.6. Theoretical calculations

All *ab initio* calculations were performed using DFT in Vienna *ab initio* simulation package (VASP) [34,35], with van der Waals density functional (vdW-DF) method [36–39] to take into account of important van der Waals interactions. All the MOF unit cells were optimized by carrying out spin-polarized calculations, with self-consistent field (SCF) convergence of 0.1 meV (1 meV = 1.6 × 10^{-22} J) and the plane wave energy cut-off set at 600 eV. The unit cell parameters and ions were allowed to move till the force acting between atoms reached below 5 meV·Å^{-1}. Potential binding sites were studied by placing CH_4, C_2H_6, and C_3H_8 molecules in MOF-303 and MIL-160 at various sites and all the atoms were allowed to relax in accordance with the convergence condition. Difference in the total energies of the MOF unit cells and the guest molecules was used to calculate the corresponding binding energies. Induced charge densities were also calculated that maps the variation in charge density upon introduction of the guest molecules and help identifying the interactions happening at the binding sites.

3. Results and discussion

3.1. Material characterization

MOF-303 and MIL-160 are built from 1D infinite chain of $[Al(OH)(COO)_2]_n$ linked through 3,5-pyrazoledicarboxylate and 2,5-furandicarboxylate, respectively, to form three-dimensional (3D) networks with straight 1D open channels, as shown in Fig. 2(a). Phase purity of the powder samples was confirmed by PXRD analysis (Fig. 2(b)). The PXRD patterns of as-synthesized samples match well with the corresponding simulated patterns. N_2 sorption experiments were conducted at 77 K to establish permanent microporosity of the samples. As shown in Figs. S1 and S2 (in Appendix A), the N_2 uptake of MOF-303 and MIL-160 increases sharply and reaches saturation at very low pressure with high adsorption capacities, indicating high microporosity of the two MOFs. MOF-303 and MIL-160 exhibit large BET surface area of 1220 and 1188 m^2·g^{-1}, respectively, and uniform micropore with size of 5–7 Å (Fig. 2(c)), which are well-suited for adsorption of C_3H_8 and C_2H_6 at low concentrations. Thermogravimetric analysis (TGA) was carried out to investigate the thermal stability of the two MOFs. As shown in Fig. S3 in Appendix A, both MOF-303 and MIL-160 show two distinct weight loss steps: The first step before 125 °C corresponds to the physically adsorbed solvent molecules, and the second step following the plateau starting from 420 and 350 °C relates to structure decomposition, indicating their high thermal stability.

3.2. Single-component adsorption isotherms of CH_4, C_2H_6, and C_3H_8

The high stability, large surface area, and especially the suitable pore diameter, as well as the high density of N or O atoms decorating the 1D channels of the two MOFs prompted us to investigate their separation performance for natural gas purification/upgrading and recovering of C_3H_8 and C_2H_6 from the gas mixture. Single-component adsorption isotherms of CH_4, C_2H_6, and C_3H_8 for MOF-303 and MIL-160 were collected at 298 K (Figs. 3(a) and (b)). Both C_3H_8 isotherms of MOF-303 and MIL-160 exhibit type I adsorption profile with very steep slopes at low pressure and reach saturation below 20 kPa, indicating strong interaction between C_3H_8 molecule and the frameworks. Notably, at 298 K and 1 bar, MOF-303 and MIL-160 adsorb 4.74 and 5.08 mmol·g^{-1} of C_3H_8, respectively. At a low pressure of 5 kPa relevant to the typical partial pressure of C_3H_8 in nature gas, the corresponding uptakes remain as high as 3.38 and 2.48 mmol·g^{-1}, much higher than those of many reported MOFs, such as University of Texas at San Antonio (UTSA)-35a [40], Fujian Institute of Research (FIR)-7a-ht [41], and MIL-100(Fe) [16], but lower than Mg/Fe/Co-MOF-74 (about 4.1 mmol·g^{-1}) [17], 0.3Gly@HKUST-1 (4.22 mmol·g^{-1}), and crystalline porous material (CPM)-734c (about 3.7 mmol·g^{-1}) [42]. This indicates the potential of MOF-303 and MIL-160 for the recovery of low pressure C_3H_8 from CH_4 stream. As shown in Figs. 3(a) and (b), the adsorption isotherms of C_2H_6 can also be characterized as

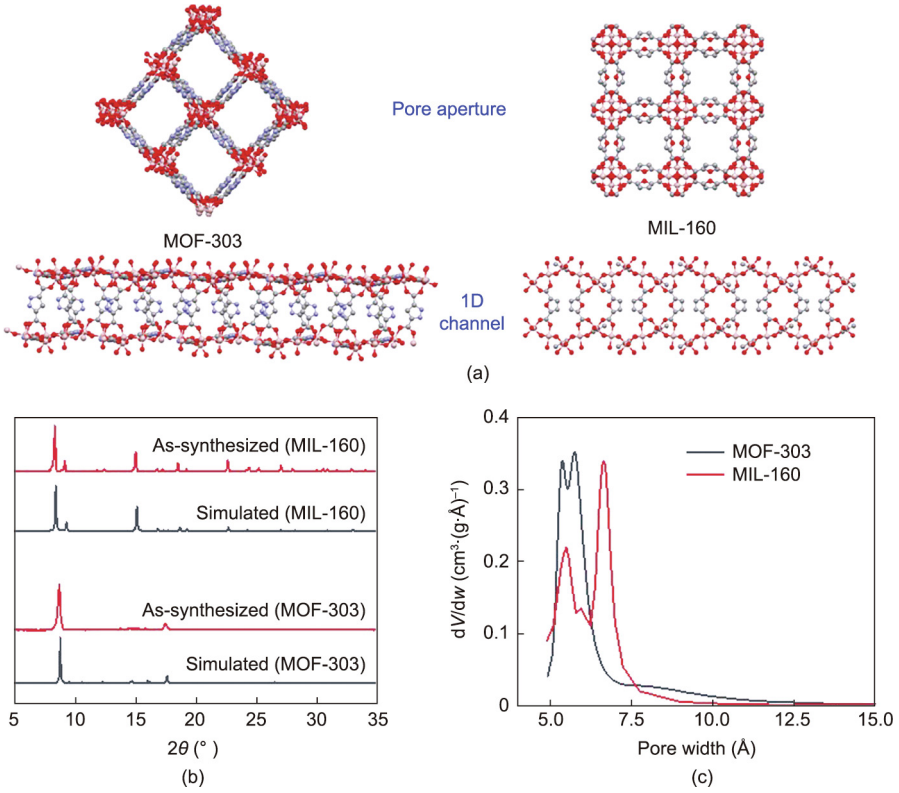

Fig. 2. (a) Pore aperture and 1D channel of MOF-303 and MIL-160. Color scheme: red, grey, pink, and light blue balls represent O, C, Al, and N atoms, respectively. (b) Experimental and simulated PXRD patterns of MOF-303 and MIL-160. (c) Pore size distribution of MOF-303 and MIL-160.

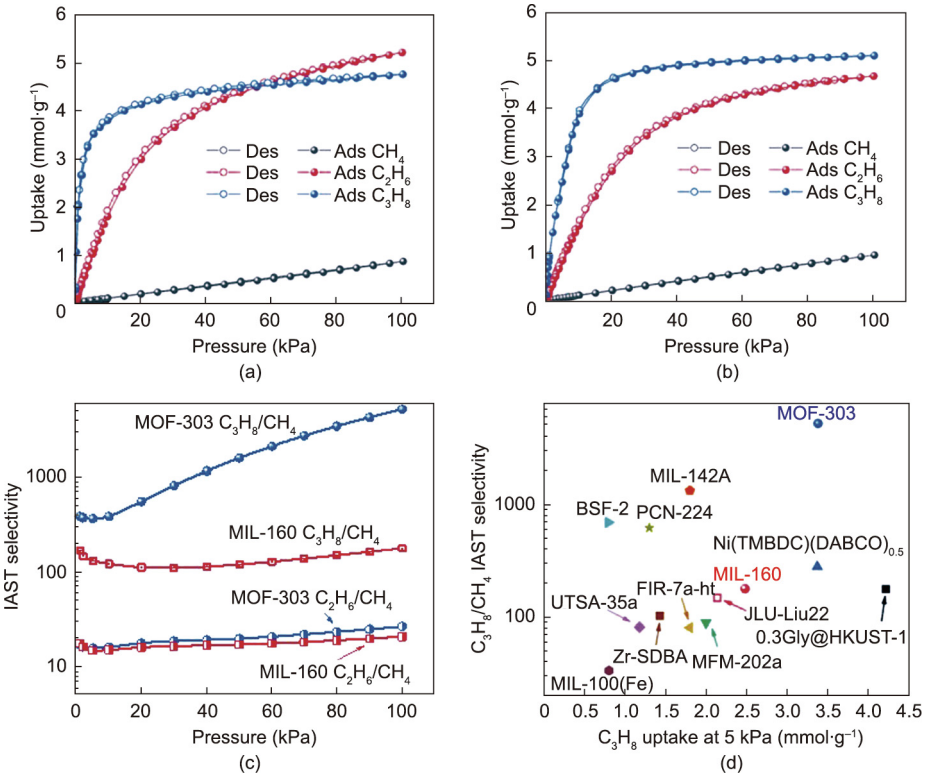

Fig. 3. Adsorption (Ads)–desorption (Des) isotherms of C_3H_8, C_2H_6, and CH_4 on (a) MOF-303 and (b) MIL-160 at 298 K. (c) IAST selectivities of MOF-303 and MIL-160 for C_3H_8/CH_4 (5:85, v/v) and C_2H_6/CH_4 (10:85, v/v) at 298 K. (d) Comparison of IAST selectivities and adsorbed amounts of C_3H_8 at 298 K and 5 kPa on MOF-303, MIL-160, and previously reported top-performing MOFs (JLU: Jilin University; MFM: Manchester framework material; H_2SDBA: 4,4′-sulfonyldibenzoic acid).

type I but with much smaller slope compared to those of C_3H_8, which may be ascribed to the weaker interaction between C_2H_6 molecule and the frameworks. The C_2H_6 uptakes are as high as 4.96 and 4.65 mmol·g^{-1} at 298 K and 1 bar for MOF-303 and MIL-160, respectively. At a relatively low pressure (10 kPa) the values are 1.59 and 1.55 mmol·g^{-1}, respectively, outperforming many reported MOFs, such as Zn-SDBA (H_2SDBA: 4,4′-sulfonyldibenzoic acid) [43], MIL-142A [44], and porous coordination network (PCN)-224 [45], except Mg/Fe/Co-MOF-74 (about 3.2 mmol·g^{-1}) [17,46], Co_2V-bdc-tpt (bdc: terephthalate; tpt: 2,4,6-tri(4-pyridyl)-1,3,5-triazine; about 2.3 mmol·g^{-1}) [47], and Ni(TMBDC)(DABCO)$_{0.5}$ (about 2.93 mmol·g^{-1}) [23]. This further confirms that the two MOFs are promising candidates for simultaneous capture of C_3H_8 and C_2H_6 from nature gas. As for CH_4, on the contrary, the isotherms are nearly straight lines with relatively low equilibrium uptake capacities of 0.86 and 0.94 mmol·g^{-1} for MOF-303 and MIL-160, respectively, suggesting weak affinity of the frameworks toward the CH_4 molecules.

To quantify the extent of interactions between the frameworks and the three hydrocarbons, isosteric heats of adsorption (Q_{st}) for CH_4, C_2H_6, and C_3H_8 were calculated (Figs. S6 and S7 in Appendix A). The zero coverage Q_{st} for MOF-303 follows the following sequence: C_3H_8 (34 kJ·mol^{-1}) > C_2H_6 (24 kJ·mol^{-1}) > CH_4 (19 kJ·mol^{-1}), which is consistent with the order of the adsorbed amounts. Similarly, for MIL-160, the Q_{st} values follow the same order: C_3H_8 (35 kJ·mol^{-1}) > C_2H_6 (28 kJ·mol^{-1}) > CH_4 (19 kJ·mol^{-1}). The apparent differences for the three gas species may result from their different polarizability and molecule size. For C_3H_8, having the highest polarizability (6.3×10^{-24} cm^3) among the three and the largest molecule dimension that is close to the pore size of the two MOFs guarantee that appreciably strong hydrogen bonds could be formed with the frameworks upon its adsorption. In contrast, CH_4 possesses a relatively low polarizability (2.6×10^{-24} cm^3) and a much smaller molecule size, leading to insufficient contacts with the pore surface and a much weaker interaction. The distinct differences in Q_{st} and adsorption capacity for CH_4, C_2H_6, and C_3H_8 make MOF-303 and MIL-160 excellent adsorbents for recovering C_3H_8 and C_2H_6 from natural gas. To more precisely evaluate the separation performance of the two MOFs under mixed-gas conditions, we calculated IAST selectivities of C_3H_8/CH_4 (5:85, v/v) and C_2H_6/CH_4 (10:85, v/v) at room temperature (298 K). As shown in Fig. 3(c), for MOF-303, the selectivity of C_3H_8/CH_4 (5:85, v/v) at 100 kPa reaches 5114, which, to the best of our knowledge, has set a new record. In addition, the selectivity for C_2H_6/CH_4 (10:85, v/v) is as high as 26, surpassing many reported MOFs (Fig. S7). Compared to MOF-303, MIL-160 possesses a similar C_2H_6/CH_4 (10:85, v/v) selectivity (20) but a much lower C_3H_8/CH_4 (5:85, v/v) selectivity (174), mainly attributed to the lower C_3H_8 uptake amount at low pressure and the slightly larger adsorbed amount of CH_4.

As a comparation, the uptake capacities of C_3H_8 and C_2H_6 combined with the C_3H_8/CH_4 and C_2H_6/CH_4 selectivities for MOF-303, MIL-160, and some representative MOFs are listed in Fig. 3(d) and Fig. S8 (in Appendix A). The C_3H_8/CH_4 selectivity of MOF-303 (5114) is the highest value reported by far and notably higher than those of top-performing MOFs, including Ni(TMBDC)-(DABCO)$_{0.5}$, BSF-2, and MIL-142A. Additionally, the C_3H_8 uptake amount (3.38 mmol·g^{-1}) is comparable to Ni(TMBDC)(DABCO)$_{0.5}$ (3.37 mmol·g^{-1}) and exceeds other MOFs, such as UTSA-35a, Manchester framework material (MFM)-202a [48], Zr-SDBA [49], and MIL-142A. For C_2H_6/CH_4, as shown in Fig. S7, MOF-303 also outperforms most of the other MOFs with higher selectivity (26) and uptake capacity (1.59 mmol·g^{-1}), such as BSF-2, ZnSDB, and UTSA-35a, but lower than that of Ni(TMBDC)(DABCO)$_{0.5}$ and Mg/Co/Fe-MOF-74 [17,46]. The ultrahigh selectivity combined with the large adsorption amount of C_3H_8 and C_2H_6 at both 100 kPa and low pressure (5 or 10 kPa) suggests that MOF-303 is of great promise for use as adsorbent in natural gas upgrading. Both the uptake amounts and selectivities of MIL-160 are slightly lower than those of MOF-303, which may be attributed to the larger pore size and the lower density of heteroatoms in MIL-160. Regardless, MIL-160 still features higher uptake and selectivity than the majority of the MOFs listed. It should be noted that while it seems MgMOF-74 and Ni(TMBDC)(DABCO)$_{0.5}$ are more promising for C_2H_6 recovery (Fig. S8) in terms of adsorption capacity and selectivity, the former suffer from low moisture resistance, and the latter is composed of an expensive ligand (TMBDC). In contrast, both MOF-303 and MIL-160 feature high thermal and moisture stability. To further confirm their outstanding hydrothermal stability, PXRD patterns of samples were collected after being treated under different conditions, including exposure to moisture for one month. As presented in Figs. S9–S12 (in Appendix A), compared to the results of as-synthesized samples, there are no notable differences found in the PXRD patterns of the samples after various treatments, confirming the excellent hydrothermal stability of both materials. As for the cost, the ligands of MOF-303 and MIL-160 are both inexpensive, and the MOFs could be readily synthesized under mild conditions. Furthermore, to assess the scale-up capability, we synthesized the two MOF sample in 5 g scale. High-quality powder products were obtained by constant stirring the mixture of ligands, aluminum salts, water, and NaOH in a glass flask at 100 °C for 12 h, with the yield higher than 90% (Figs. S13–S18 in Appendix A). The high moisture stability, low cost, and the facile scale-up capability further corroborate the feasibility for the implementation of MOF-303 and MIL-160 in industrial separation technology.

3.3. Density functional theory analysis

To understand the gas adsorption behavior and mechanism in MOF-303 and MIL-160, DFT calculations were performed on both structures. As shown in Figs. 4(a)–(c), all three guest molecules at their primary binding positions occupy similar sites in the pore of MOF-303. The binding energy calculations show a binding strength order of C_3H_8 (60.1 kJ·mol^{-1}) > C_2H_6 (47.4 kJ·mol^{-1}) > CH_4 (30.7 kJ·mol^{-1}) at their primary binding sites located near the MOF linker. This result agrees with the experimental uptake trends for MOF-303 at low pressures. The induced charge density for the three gas molecules (Figs. 4(d)–(f)) shows most charge rearrangement occurring between the guest molecules and the N atoms in the linker, confirming that the N atoms are the strongest binding sites in MOF-303. As shown in Figs. 4(c) and (f), the highest binding energy and induced charge density for C_3H_8 are likely a result of its longer C3 chain, larger kinetic diameter, and a greater number of C–H arms as compared with C_2H_6 and CH_4, which enable it to interact more closely with multiple linkers and form multiple stronger hydrogen bonds. The charge rearrangements for MIL-160 are shown in Fig. S19 (in Appendix A). All three guest molecules prefer binding near the linkers and interact primarily with the O atoms on both the furan ring and the carboxyl groups via their C–H bonds. Different from their binding sites in MOF-303, CH_4 and C_2H_6 molecules bind close to linkers on one side of pore (Figs. S19(d) and (e)), which may be attributed to the larger pore size of MIL-160 (Fig. 2(c)). On the other hand, C_3H_8, owing to its larger size, occupies a more central position in the pore and interacts with linkers on three different sides. The binding energy calculations for MIL-160 generate the same trend as that of MOF-303, with the descending order of C_3H_8 (65.7 kJ·mol^{-1}) > C_2H_6 (55.8 kJ·mol^{-1}) > CH_4 (34.9 kJ·mol^{-1}) at the primary binding site (Figs. S19(a)–(c)), in consistent with the experimental observations.

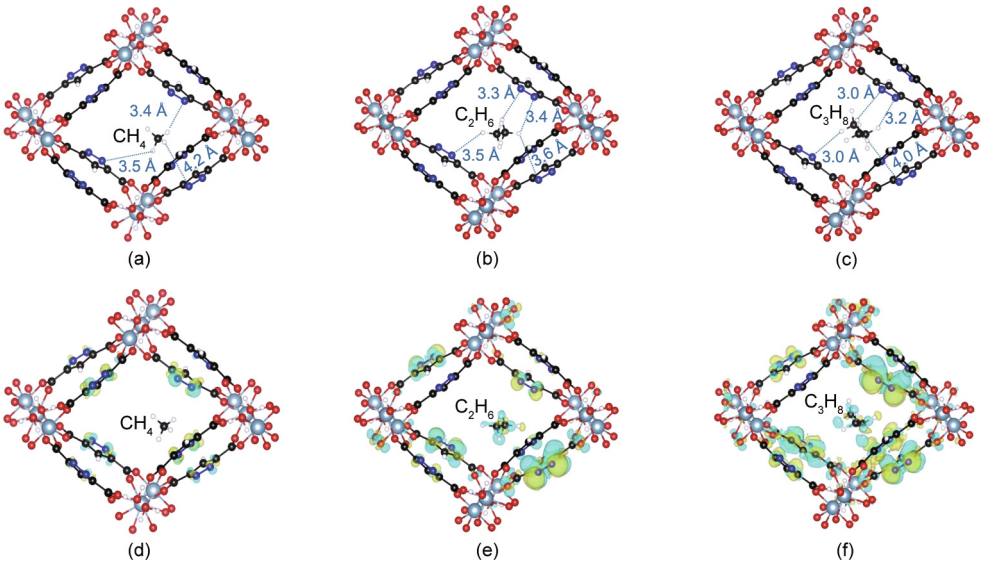

Fig. 4. The unit cell of MOF-303 used for calculating binding energies. (a–c) The results for (a) CH_4, (b) C_2H_6, and (c) C_3H_8 show their primary binding site (color scheme: silver, red, black, blue, and white balls represent Al, O, C, N, and H). (d–f) Induced charge densities for (d) CH_4, (e) C_2H_6, and (f) C_3H_8 (iso-level is 0.001 electrons·Å^{-3}). Blue highlighted areas represent a depletion of charge and yellow areas represent an increase in charge after the guest molecule occupies a binding site.

3.4. Breakthrough experiments, adsorbent regeneration, and recyclability tests

To further evaluate the actual separation potential of MOF-303 and MIL-160, dynamic breakthrough experiments were carried out on ternary ($CH_4/C_2H_6/C_3H_8$, 85:10:5, v/v/v) gas mixtures at 298 K. For the breakthrough curves of MOF-303, as shown in Fig. 5(a), CH_4 eluted out first at 15 min·g^{-1}, followed by C_2H_6 and C_3H_8 with a breakthrough time of 120 and 760 min·g^{-1}, respectively, coinciding well with the order of static capacities and isosteric heats. The distinct breakthrough times for the three gases confirm that MOF-303 can afford efficient natural gas upgrading by the individual C_3H_8 and C_2H_6 recovery (as shown in Fig. S20 in Appendix A). The breakthrough curves of MIL-160 are similar to those of MOF-303 but exhibit a much shorter breakthrough time for C_3H_8 (388 min·g^{-1}), as shown in Fig. 5(b), which is consistent with the lower

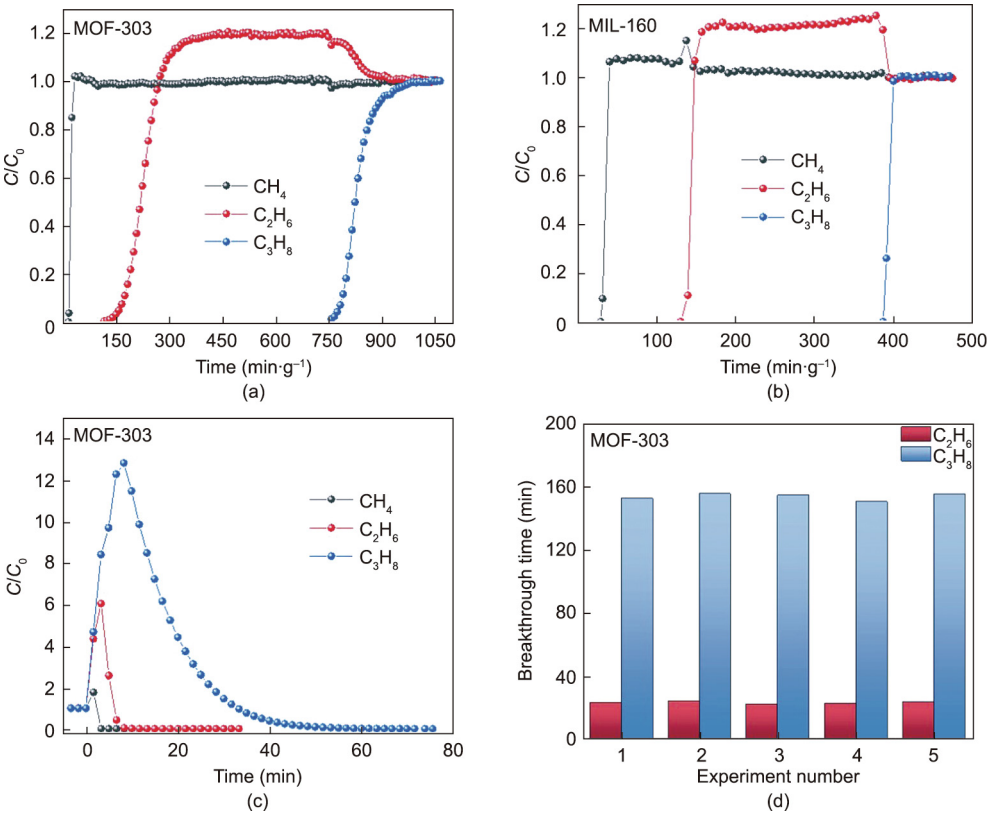

Fig. 5. (a, b) Ternary breakthrough curves ($CH_4/C_2H_6/C_3H_8$, 85:10:5, v/v/v) of (a) MOF-303 and (b) MIL-160 at 298 K. (c) Desorption curves of MOF-303 packed column at 333 K under 5 mL·min^{-1} N_2 flow. (d) C_3H_8 and C_2H_6 breakthrough times of MOF-303 in consecutive five cycles of breakthrough experiments (298 K and 100 kPa).

static adsorption capacity of MIL-160 for C_3H_8 at 5 kPa. To evaluate the regeneration property of MOF-303 and MIL-160, desorption was carried out under dynamic N_2 flowing at 333 K. As shown in Fig. 5(c), during the desorption process for MOF-303, CH_4, C_2H_6, and C_3H_8 can be fully removed in 4, 12, and 50 min, respectively, demonstrating that MOF-303 column can be fully regenerated under mild condition. Finally, five breakthrough measurements were carried out consecutively to evaluate the recycling performance of MOF-303 and MIL-160. As illustrated in Fig. 5(d) and Fig. S21 (in Appendix A), the breakthrough times for C_3H_8 and C_2H_6 are nearly constant, suggesting good recyclability of both adsorbents.

4. Conclusion

In summary, two highly stable Al-based MOFs, MOF-303 and MIL-160, have been investigated for efficient separation and recovery of C_2H_6 and C_3H_8 from natural gas. The large surface area, suitable pore diameter, and the high density of N or O atoms in the 1D open channels synergistically enhance the affinity of the frameworks toward C_3H_8 and C_2H_6, resulting in large uptake capacity and excellent selectivity. In particular, for MOF-303, the uptake of C_3H_8 at 298 K and 5 kPa is up to 3.38 mmol·g^{-1} along with a record-high IAST selectivity of 5114 for C_3H_8/CH_4 (5:85, v/v). MOF-303 also possesses high adsorption capacity for C_2H_6 (at 10 kPa) and high C_2H_6/CH_4 (10:85, v/v) selectivity, reaching values of 1.59 mmol·g^{-1} and 26, respectively. DFT calculations verified that the strong affinity between C_3H_8 (or C_2H_6) molecules and the heteroatoms on the linkers gives rise to the high loading capacity and selectivity for C_3H_8 and C_2H_6. To investigate the potential of using MOF-303 and MIL-160 to upgrade natural gas and to recover C_3H_8 and C_2H_6, further experiments, including hydrothermal stability and scale-up capability tests, as well as breakthrough experiments, were carried out on both MOFs. The stability tests revealed their exceptional resistance to moisture. The scale-up capabilities were verified through reactions at 5 g scale with quantitative yields. Finally, ternary breakthrough experiments and recyclability tests further confirmed the great potential of MOF-303 and MIL-160 as advanced adsorbents for efficient separation of $C_3H_8/C_2H_6/CH_4$.

Acknowledgment

We would like to thank the US Department of Energy, Office of Science, Office of Basic Energy Sciences (DE-SC0019902) for the partial support of this work. Shikai Xian, Junjie Peng, and Hao Wang acknowledge the financial support from National Natural Science Foundation of China (21908069 and 21901166), Guangdong Natural Science Foundation (2019A1515010692), and Shenzhen Science and Technology Program (JCYJ20190809145615620 and RCYX20200714114539243).

Compliance with ethics guidelines

Shikai Xian, Junjie Peng, Haardik Pandey, Timo Thonhauser, Hao Wang, and Jing Li declare that they have no conflict of interest or financial conflicts to disclose.

Appendix A. Supplementary data

Supplementary data to this article can be found online at https://doi.org/10.1016/j.eng.2022.07.017.

References

[1] He Y, Zhou W, Qian G, Chen B. Methane storage in metal–organic frameworks. Chem Soc Rev 2014;43(16):5657–78.
[2] Sholl DS, Lively RP. Seven chemical separations to change the world. Nature 2016;532(7600):435–7. Corrected in: Nature 2016;533(7603):316.
[3] Baker RW, Lokhandwala K. Natural gas processing with membranes: an overview. Ind Eng Chem Res 2008;47(7):2109–21.
[4] Mason JA, Veenstra M, Long JR. Evaluating metal–organic frameworks for natural gas storage. Chem Sci 2014;5(1):32–51.
[5] Estupiñan Perez L, Avila AM, Sawada JA, Rajendran A, Kuznicki SM. Process optimization-based adsorbent selection for ethane recovery from residue gas. Separ Purif Tech 2016;168:19–31.
[6] Plonka AM, Chen X, Wang H, Krishna R, Dong X, Banerjee D, et al. Light hydrocarbon adsorption mechanisms in two calcium-based microporous metal organic frameworks. Chem Mater 2016;28(6):1636–46.
[7] Li L, Wang X, Liang J, Huang Y, Li H, Lin Z, et al. Water-stable anionic metal–organic framework for highly selective separation of methane from natural gas and pyrolysis gas. ACS Appl Mater Interfaces 2016;8(15):9777–81.
[8] Ruthven DM. Past progress and future challenges in adsorption research. Ind Eng Chem Res 2000;39(7):2127–31.
[9] Liang W, Xiao H, Lv D, Xiao J, Li Z. Novel asphalt-based carbon adsorbents with super-high adsorption capacity and excellent selectivity for separation for light hydrocarbons. Sep Purif Technol 2018;190:60–7.
[10] Zhao X, Wang Y, Li DS, Bu X, Feng P. Metal–organic frameworks for separation. Adv Mater 2018;30(37):1705189.
[11] Cui WG, Hu TL, Bu XH. Metal–organic framework materials for the separation and purification of light hydrocarbons. Adv Mater 2020;32(3):1806445.
[12] Zhai QG, Bu X, Zhao X, Li DS, Feng P. Pore space partition in metal–organic frameworks. Acc Chem Res 2017;50(2):407–17.
[13] Yang SQ, Sun FZ, Krishna R, Zhang Q, Zhou L, Zhang YH, et al. Propane-trapping ultramicroporous metal–organic framework in the low-pressure area toward the purification of propylene. ACS Appl Mater Interfaces 2021;13(30):35990–6.
[14] Yu MH, Space B, Franz D, Zhou W, He C, Li L, et al. Enhanced gas uptake in a microporous metal–organic framework via a sorbate induced-fit mechanism. J Am Chem Soc 2019;141(44):17703–12.
[15] Zhang Y, Yang L, Wang L, Cui X, Xing H. Pillar iodination in functional boron cage hybrid supramolecular frameworks for high performance separation of light hydrocarbons. J Mater Chem A 2019;7(48):27560–6.
[16] Yuan B, Wang X, Zhou X, Xiao J, Li Z. Novel room-temperature synthesis of MIL-100(Fe) and its excellent adsorption performances for separation of light hydrocarbons. Chem Eng J 2019;355:679–86.
[17] He Y, Krishna R, Chen B. Metal–organic frameworks with potential for energy-efficient adsorptive separation of light hydrocarbons. Energy Environ Sci 2012;5(10):9107–20.
[18] Wu Y, Sun Y, Xiao J, Wang X, Li Z. Glycine-modified HKUST-1 with simultaneously enhanced moisture stability and improved adsorption for light hydrocarbons separation. ACS Sustain Chem Eng 2019;7(1):1557–63.
[19] DeCoste JB, Peterson GW, Schindler BJ, Killops KL, Browe MA, Mahle JJ. The effect of water adsorption on the structure of the carboxylate containing metal–organic frameworks Cu-BTC, Mg-MOF-74, and UiO-66. J Mater Chem A 2013;1(38):11922–32.
[20] Xian S, Peng J, Zhang Z, Xia Q, Wang H, Li Z. Highly enhanced and weakened adsorption properties of two MOFs by water vapor for separation of CO_2/CH_4 and CO_2/N_2 binary mixtures. Chem Eng J 2015;270:385–92.
[21] Xian S, Wu Y, Wu J, Wang X, Xiao J. Enhanced dynamic CO_2 adsorption capacity and CO_2/CH_4 selectivity on polyethylenimine-impregnated UiO-66. Ind Eng Chem Res 2015;54(44):11151–8.
[22] Wang S, Serre C. Toward green production of water-stable metal–organic frameworks based on high-valence metals with low toxicities. ACS Sustain Chem Eng 2019;7(14):11911–27.
[23] Wu Y, Liu Z, Peng J, Wang X, Zhou X, Li Z. Enhancing selective adsorption in a robust pillared-layer metal–organic framework via channel methylation for the recovery of C2–C3 from natural gas. ACS Appl Mater Interfaces 2020;12(46):51499–505.
[24] Silva P, Vilela SMF, Tomé JPC, Almeida Paz FA. Multifunctional metal–organic frameworks: from academia to industrial applications. Chem Soc Rev 2015;44(19):6774–803.
[25] Czaja A, Leung E, Trukhan N, Müller U. Industrial MOF synthesis. In: Farrusseng D, editor. Metal–organic frameworks: applications from catalysis to gas storage. Weinheim: Wiley-VCH Verlag & Co. KGaA; 2011. p. 337–52.
[26] Ye Y, Xian S, Cui H, Tan K, Gong L, Liang B, et al. Metal–organic framework based hydrogen-bonding nanotrap for efficient acetylene storage and separation. J Am Chem Soc 2022;144(4):1681–9.
[27] Yang L, Qian S, Wang X, Cui X, Chen B, Xing H. Energy-efficient separation alternatives: metal–organic frameworks and membranes for hydrocarbon separation. Chem Soc Rev 2020;49(15):5359–406.
[28] Devic T, Serre C. High valence 3p and transition metal based MOFs. Chem Soc Rev 2014;43(16):6097–115.
[29] Yuan S, Qin JS, Lollar CT, Zhou HC. Stable metal–organic frameworks with group 4 metals: current status and trends. ACS Cent Sci 2018;4(4):440–50.
[30] Yang H, Peng F, Hong AN, Wang Y, Bu X, Feng P. Ultrastable high-connected chromium metal–organic frameworks. J Am Chem Soc 2021;143(36):14470–4.

[31] He T, Kong XJ, Li JR. Chemically stable metal–organic frameworks: rational construction and application expansion. Acc Chem Res 2021;54(15):3083–94.
[32] Kong XJ, Li JR. An overview of metal–organic frameworks for green chemical engineering. Engineering 2021;7(8):1115–39.
[33] Fathieh F, Kalmutzki MJ, Kapustin EA, Waller PJ, Yang J, Yaghi OM. Practical water production from desert air. Sci Adv 2018;4(6):eaat3198.
[34] Kresse G, Furthmüller J. Efficient iterative schemes for *ab initio* total-energy calculations using a plane-wave basis set. Phys Rev B 1996;54(16):11169–86.
[35] Kresse G, Joubert D. From ultrasoft pseudopotentials to the projector augmented-wave method. Phys Rev B 1999;59(3):1758–75.
[36] Berland K, Cooper VR, Lee K, Schröder E, Thonhauser T, Hyldgaard P, et al. Van der Waals forces in density functional theory: a review of the vdW-DF method. Rep Prog Phys 2015;78(6):066501.
[37] Langreth DC, Lundqvist BI, Chakarova-Käck SD, Cooper VR, Dion M, Hyldgaard P, et al. A density functional for sparse matter. J Phys Condens Matter 2009;21(8):084203.
[38] Thonhauser T, Cooper VR, Li S, Puzder A, Hyldgaard P, Langreth DC. Van der Waals density functional: self-consistent potential and the nature of the van der Waals bond. Phys Rev B 2007;76(12):125112.
[39] Thonhauser T, Zuluaga S, Arter CA, Berland K, Schröder E, Hyldgaard P. Spin signature of nonlocal correlation binding in metal–organic frameworks. Phys Rev Lett 2015;115(13):136402.
[40] He Y, Zhang Z, Xiang S, Fronczek FR, Krishna R, Chen B. A robust doubly interpenetrated metal–organic framework constructed from a novel aromatic tricarboxylate for highly selective separation of small hydrocarbons. Chem Commun 2012;48(52):6493–5.
[41] He YP, Tan YX, Zhang J. Tuning a layer to a pillared-layer metal–organic framework for adsorption and separation of light hydrocarbons. Chem Commun 2013;49(96):11323–5.
[42] Hong AN, Yang H, Li T, Wang Y, Wang Y, Jia X, et al. Pore-space partition and optimization for propane-selective high-performance propane/propylene separation. ACS Appl Mater Interfaces 2021;13(44):52160–6.
[43] Tang FS, Lin RB, Lin RG, Zhao JCG, Chen B. Separation of C2 hydrocarbons from methane in a microporous metal–organic framework. J Solid State Chem 2018;258:346–50.
[44] Yuan Y, Wu H, Xu Y, Lv D, Tu S, Wu Y, et al. Selective extraction of methane from C1/C2/C3 on moisture-resistant MIL-142A with interpenetrated networks. Chem Eng J 2020;395:125057.
[45] Shi R, Lv D, Chen Y, Wu H, Liu B, Xia Q, et al. Highly selective adsorption separation of light hydrocarbons with a porphyrinic zirconium metal–organic framework PCN-224. Sep Purif Technol 2018;207:262–8.
[46] Bloch ED, Queen WL, Krishna R, Zadrozny JM, Brown CM, Long JR. Hydrocarbon separations in a metal–organic framework with open iron(II) coordination sites. Science 2012;335(6076):1606–10.
[47] Yang H, Wang Y, Krishna R, Jia X, Wang Y, Hong AN, et al. Pore-space-partition-enabled exceptional ethane uptake and ethane-selective ethane–ethylene separation. J Am Chem Soc 2020;142(5):2222–7.
[48] Gao S, Morris CG, Lu Z, Yan Y, Godfrey HGW, Murray C, et al. Selective hysteretic sorption of light hydrocarbons in a flexible metal–organic framework material. Chem Mater 2016;28(7):2331–40.
[49] Gu J, Sun X, Kan L, Qiao J, Li G, Liu Y. Structural regulation and light hydrocarbon adsorption/separation of three zirconium–organic frameworks based on different V-shaped ligands. ACS Appl Mater Interfaces 2021;13(35):41680–7.